

Electronic Stopping and Momentum Density of Diamond Obtained from First-Principles Calculations

Richard J. Mathar*

Goethestr. 22, 69151 Neckargemünd, Germany

(Dated: November 19, 2018)

We calculate the “head” element or the $(\mathbf{0}, \mathbf{0})$ -element of the wave-vector and frequency-dependent dielectric matrix of bulk crystals via first-principles, all-electron Kohn-Sham states in the integral of the irreducible polarizability in the random phase approximation. We approximate the macroscopic “head” element of the inverse matrix by its reciprocal value, and integrate over frequencies and momenta to obtain the electronic energy loss of protons at low velocities. Numerical evaluation for diamond targets predicts that the band gap causes a strong non-linear reduction of the electronic stopping power at ion velocities below 0.2 atomic units.

PACS numbers: 61.80.Jh, 34.50.Bw, 71.45.Gm

I. FORMULATION AND METHOD

The objective of this research is a quantitative, first-principles description of the energy deposition by a bare ion in diamond. The energy loss per unit path length of a massive, punctiform, charged particle with charge number Z_1 to a target is¹

$$\frac{dE}{dx}(\mathbf{v}) = \frac{(Z_1 e)^2}{4\pi^3 \epsilon_0 v} \int d^3 q \frac{\mathbf{v} \cdot \mathbf{q}}{q^2} \int_0^\infty d\omega \delta(\omega - \mathbf{q} \cdot \mathbf{v}) \text{Im} K_{\mathbf{0}, \mathbf{0}}(\mathbf{q}, \omega), \quad (1)$$

with \mathbf{v} the projectile velocity in the target rest frame, e the elementary charge unit, and ϵ_0 the vacuum permittivity. For reciprocal lattice vectors \mathbf{G} , $K_{\mathbf{0}, \mathbf{0}}$ is the $\mathbf{G} = \mathbf{G}' = \mathbf{0}$ (“head”) component of the inverse dielectric matrix defined by

$$\sum_{\mathbf{G}'} \epsilon_{\mathbf{G}, \mathbf{G}'}(\mathbf{q}, \omega) K_{\mathbf{G}', \mathbf{G}''}(\mathbf{q}, \omega) = \delta_{\mathbf{G} \mathbf{G}''}$$

with respect to $\epsilon_{\mathbf{G}, \mathbf{G}'}(\mathbf{k}, \omega)$, the wave-vector and frequency dependent microscopic dielectric matrix. In terms of the irreducible polarizability Π , the dielectric matrix is

$$\epsilon_{\mathbf{G}, \mathbf{G}'}(\mathbf{q}, \omega) = \delta_{\mathbf{G} \mathbf{G}'} - \frac{e^2}{\epsilon_0 |\mathbf{q} + \mathbf{G}|^2} \Pi(\mathbf{q} + \mathbf{G}, \mathbf{q} + \mathbf{G}', \omega),$$

given in the Random Phase Approximation² (RPA) as a sum over all band pairs (ν, ν') and an integral over the first Brillouin zone (BZ)

$$\begin{aligned} & \Pi(\mathbf{q} + \mathbf{G}, \mathbf{q} + \mathbf{G}', \omega) \\ &= \sum_{\nu \nu'} \int_{\text{BZ}} \frac{d^3 k}{(2\pi)^3} \frac{m_{\mathbf{G}}^* m_{\mathbf{G}'}}{\hbar \omega + i\eta + E_{\nu \mathbf{k}} - E_{\nu' \mathbf{k} + \mathbf{q}}}. \end{aligned} \quad (2)$$

$E_{\nu, \mathbf{k}}$ are the band energies, and $f_{\nu, \mathbf{k}}$ are Fermi occupation numbers ($f_{\nu, \mathbf{k}} = 0$ or 2 for $E_{\nu, \mathbf{k}}$ above or below the Fermi energy E_F). The matrix elements in Eq. (2) are

$$m_{\mathbf{G}} \equiv \langle \nu' \mathbf{k} + \mathbf{q} | e^{i(\mathbf{G} + \mathbf{q}) \cdot \mathbf{r}} | \nu \mathbf{k} \rangle.$$

We determine the ground-state electronic structure of solids within Density Functional Theory (DFT) as established in the Kohn-Sham (KS) variational procedure and implemented in the computational package GTOFF.³ The results of the all-electron, full-potential calculations are eigenfunctions $\varphi_{\nu, \mathbf{k}}(\mathbf{r})$, expressed as linear combination of Gaussian Type Orbitals (GTO's), and eigenvalues $E_{\nu, \mathbf{k}}$.

The Bloch functions are finally expanded in a (truncated) plane wave (PW) series,

$$\varphi_{\nu, \mathbf{k}} = \langle \mathbf{r} | \nu \mathbf{k} \rangle = e^{i\mathbf{k} \cdot \mathbf{r}} u_{\nu \mathbf{k}}(\mathbf{r}) = \frac{1}{V_{\text{UC}}} \sum_{\mathbf{G}} e^{i(\mathbf{k} + \mathbf{G}) \cdot \mathbf{r}} u_{\nu \mathbf{k}, \mathbf{G}},$$

to represent $m_{\mathbf{G}}$ as a simple sum over products of expansion coefficients $u_{\nu \mathbf{k}, \mathbf{G}}$,¹ where V_{UC} is the volume of a unit cell (UC). The equivalence of the GTO and PW representations is maintained by monitoring the accumulated norm for each $|\nu, \mathbf{k}\rangle$ relative to the exact values,

$$\sum_{\mathbf{G}} |u_{\nu, \mathbf{k}, \mathbf{G}}|^2 = V_{\text{UC}}. \quad (3)$$

We subdivide the integration region of the integral (2) into \mathbf{k} -space tetrahedra. Recursive further subdivision of a given tetrahedron into smaller tetrahedra is done if $f_{\nu \mathbf{k}} - f_{\nu' \mathbf{k} + \mathbf{q}}$ is not constant over all four vertices. Next comes linearization of the product of the matrix elements in the numerator and of the energy denominator inside each tetrahedron for each ω . The resulting approximated integral is evaluated analytically.¹

The product $|\mathbf{q} + \mathbf{G}|^2 \epsilon_{\mathbf{G}, \mathbf{G}'}(\mathbf{q}, \omega)$ is calculated and, in compensation, the term q^2 in the denominator of Eq. (1) is dropped. The dielectric function is tabulated for \mathbf{q} commensurate with the uniform mesh of wave vectors used in the underlying GTOFF calculation but covering higher BZ's as well as the first. [Values outside the (\mathbf{q}, ω) -meshes are replaced by the vacuum response, $\text{Im} K_{\mathbf{0}, \mathbf{0}}(\mathbf{q}, \omega) = 0$.] $\text{Im} K_{\mathbf{G}, \mathbf{G}'}$ is linearized inside each \mathbf{q} -space tetrahedron. Multiplied by the linear factor $\mathbf{q} \cdot \mathbf{v}$, the integrals (1) over tetrahedra are done analytically, then summed.

II. DIAMOND

A. Basis Sets, Electron Momentum Density

Diamond is studied at the experimental lattice parameter, $a = 6.74071a_0$ for the cubic unit cell, where a_0 denotes one bohr. The Moruzzi-Janak-Williams parameterization⁴ of the Hedin-Lundqvist local-density approximation (LDA) to the exchange-correlation potential is used. Small, highly contracted basis sets as used in Ref. 5 are generally insufficient to calculate the real parts of dielectric functions and subsequently the energy loss functions. We started from Partridge's 16s11p set,⁶ contracted the seven tightest s -functions and the four tightest p -functions, removed the most diffuse s and the two most diffuse p -functions to avoid approximate linear dependencies, and added a full set of three d -functions with exponents equal to the remaining most diffuse p -functions. (Without d -orbitals the total energy would rise by 0.24 eV/atom.) Site centered s - and f -type fitting functions were used with exponents for the s -types as in Ref. 7, and for the f -types $0.5/a_0^2$ and $0.2/a_0^2$ as in Ref. 8. Space group and lattice type are those of silicon; hence we may refer to a prior GTOFF study⁹ for the symmetry properties of the fitting functions.

The density of states (DOS) computed with this 9s6p3d basis (84 basis functions in the primitive UC) as shown in Fig. 1 is stable up to ≈ 70 eV above the Fermi energy with respect to further de-contraction. Band gaps are too small compared with experiments, as usual for the LDA and known from other DFT calculations on diamond.¹⁰

The lowest 24 bands were expanded into 531 plane waves, a cut-off at $|\mathbf{G}| = 7.3/a_0$, with a norm in Eq. (3) above $0.85V_{UC}$ for the K -shell electrons (excitations from which were excluded in the subsequent calculations of $\epsilon_{\mathbf{G},\mathbf{G}'}$ and dE/dx anyway), and a norm above $0.98V_{UC}$ for the remaining 22 bands. A first result is the all-electron momentum density (EMD)

$$\rho(\mathbf{k} + \mathbf{G}) \equiv \frac{1}{V_{UC}} \sum_{\nu} f_{\nu,\mathbf{k}} |u_{\nu,\mathbf{k},\mathbf{G}}|^2$$

in Fig. 2. The values near zero momentum $\mathbf{k} + \mathbf{G} = 0$ are the states with long wavelengths and reveal the macroscopic symmetry of the crystal system, the 4-fold axis of the cubic system here. If $|\mathbf{k} + \mathbf{G}|$ is of the order of half a reciprocal lattice vector, the interference with the next nearest neighbors in the lattice becomes visible; the eight foothills in the figure may be interpreted as a projection of the four corners of a carbon tetrahedron onto the (001) plane complemented by the inversion¹¹

$$u_{\nu,-\mathbf{k},-\mathbf{G}} = u_{\nu,\mathbf{k},\mathbf{G}}^*$$

If $|\mathbf{k} + \mathbf{G}|$ is large, the spherical symmetry of the core states prevails.

B. Dielectric Function

The element $\epsilon_{0,0}(\mathbf{q}, \omega)$ of the dielectric matrix is shown in Fig. 3. The main absorption peak at 11 eV for $|\mathbf{q}| \rightarrow 0$ corresponds to direct transitions from the top of the valence to the bottom of the conduction band at X and L.¹²

Local Field Effects are illustrated in Fig. 4. $\text{Im}\epsilon_{0,0}$ repeats some values of Fig. 3; $\text{Im}[1/K_{0,0}]$ includes an estimate of the local field by calculating $K_{\mathbf{G},\mathbf{G}'}$ as the inverse of a 9×9 dielectric matrix which contains $\mathbf{G} = 0$ and the eight vectors of the closest shell in the bcc reciprocal lattice. The reduction of the values without LFE ($|\text{Im}\epsilon_{0,0}|$, open symbols) compared to those with LFE ($|\text{Im}(1/K_{0,0})|$, filled symbols) is of the order reported by Van Vechten and Martin¹³ (without their ‘‘dynamical correlations’’). The different sign of the effect for frequencies above and below the peak has been noticed before.¹⁴ The differences are even smaller for the energy loss function. Hence the energy loss in the next paragraph was calculated from $\epsilon_{0,0}(\mathbf{q}, \omega)$ alone.

C. Computed Electronic Energy Loss

To integrate the energy loss function as described by Eq. (1), the BZ mesh was reduced to $8 \times 8 \times 8$ points, i.e., 35 points in the irreducible Brillouin zone (IBZ). The result is shown in Fig. 5. The dielectric matrix was tabulated on a $30 \times 30 \times 30$ mesh in \mathbf{q} -space (parallelepiped with three edges of length $6.1/a_0$), and the stopping power was integrated over the superset of all \mathbf{q} -values obtained from these via point group operations with Seitz symbol $\{O|\mathbf{w}\}$,

$$K_{\mathbf{G},\mathbf{G}'}(\mathbf{q}, \omega) = e^{iO(\mathbf{G}-\mathbf{G}')\cdot\mathbf{w}} K_{O\mathbf{G},O\mathbf{G}'}(O\mathbf{q}, \omega).$$

It is about 0–15% lower than experimental results¹⁵ for $v \approx 1 \dots 1.3v_0$ which are shown in Fig. 6. ($v_0 \approx 2.19 \cdot 10^6$ m/s is one atomic unit of velocity. Values within the LPDA represent integrals of the all-electron density of GTOFF Fitting Functions weighted with the stopping number of the FEG in the RPA.) Reduction of the integrated \mathbf{q} -region to the parallelepiped decreases the stopping cross section by approximately 10% at $v \approx v_0$.¹⁶ Within the framework of linear dielectric response an underestimation is appropriate though, because terms of $O(Z_1^3)$ will add about 15% to $S(v)$ at $v \approx 1.5v_0$.¹⁷

A new result is the ‘‘ionic’’ band gap, the non-linear suppression of $S(v)$ for $v \lesssim 0.2v_0$, which is approximately the value extracted from¹⁶

$$v < \frac{v_0}{2} \sqrt{\hbar\omega_g/E_0} \quad (4)$$

for a band gap of $\hbar\omega_g = 4$ eV. (E_0 is one rydberg.) By way of contrast, calculations within the local-plasma-density approximation usually integrate over volume elements in real space that are parameterized by the homogeneous electron gas, and inevitably yield $S(v) \propto v$ at

low velocities. However, an attempt at experimental verification of this reduction of the energy loss in a wide-gap material is handicapped by the additional nuclear energy loss, which has an estimated maximum of $S \approx 0.8 \cdot 10^{-15}$ eVcm²/atoms at $v \approx 0.08v_0$.¹⁸

Note that Eq. (4) predicts contributions from *K*-shell excitations to start at $v \approx 2.2v_0$, which are not included here. They have been estimated to shift the maximum to higher velocities by about $0.2v_0$,¹⁹ and to grow until $v \approx 5.3v_0$.²⁰

Acknowledgments

Helpful conversations with S.B. Trickey and J.R. Sabin are gratefully acknowledged. This work was supported by grant DAA-H04-95-1-0326 from the U.S. Army Research Office.

-
- * Electronic address: mathar@mpia-hd.mpg.de
- ¹ For a thorough discussion of the underlying approximations (linear response, neglect of channeling and local field factors etc.) and the implementation see R.J. Mathar, S.B. Trickey, and J.R. Sabin, Nucl. Instrum. Methods B **155**, 249 (1999); 17th Werner Brandt Workshop on Charged Particle Penetration Phenomena, May 8–9, 1997, Charlottesville, VA (unpublished).
 - ² S.L. Adler, Phys. Rev. **126**, 413 (1962). Eqs. (2.11)–(2.12) are inconsistent with eqs. (2.7)–(2.10). Either fields ϕ must be replaced by charge densities ρ in (2.11)–(2.12), or all factors of squared wavenumbers be dropped.
 - ³ J.C. Boettger and S.B. Trickey, Phys. Rev. B **53**, 3007 (1996); J.C. Boettger and J.M. Wills, *ibid.* **54**, 8965 (1996); J.C. Boettger, *ibid.* **55**, 750 (1997); **55**, 11202 (1997).
 - ⁴ V.L. Moruzzi, J.F. Janak, and A.R. Williams, *Calculated Electronic Properties of Metals*, (Pergamon, New York, 1978).
 - ⁵ D. Ayma, J.P. Campillo, M. Rérat, and M. Causà, J. Comput. Chem. **18**, 1253 (1997); D. Ayma, M. Rérat, and A. Lichanot, J. Phys. Condens. Matter **10**, 557 (1998).
 - ⁶ H. Partridge, National Aeronautics and Space Administration (NASA) Technical Memorandum 1.15:101044, Ames Research Center, Moffet Field, 1989.
 - ⁷ S.B. Trickey, F. Müller-Plathe, and G.H.F. Diercksen, Phys. Rev. B **45**, 4460 (1992).
 - ⁸ Because no bond-centered basis functions are used, the charge fitting functions do not reproduce the quasi-forbidden (222) X-ray reflex: Z.W. Lu, A. Zunger, and M. Deutsch, Phys. Rev. B **47**, 9385 (1993); M.A. Spackman, Acta Crystallogr. Sect. A **47**, 420 (1991); T. Takama, K. Tsuchiya, K. Kobayashi, and S. Sato, *ibid.* **46**, 514 (1990).
 - ⁹ J.C. Boettger, Int. J. Quantum Chem. **60**, 1345 (1996).
 - ¹⁰ S. Fahy, X.W. Wang, and S.G. Louie, Phys. Rev. Lett. **61**, 1631 (1988); M.R. Salehpour and S. Satpathy, Phys. Rev. B **41**, 3048 (1990); A. Onodera, M. Hasegawa, K. Furuno, M. Kobayashi, Y. Nisida, H. Sumiya, and S. Yazu, *ibid.* **44**, 12176 (1991); M.P. Surh, S.G. Louie, and M.L. Cohen, *ibid.* **45**, 8239 (1992); S. Logothetidis, J. Petalas, H.M. Polatoglou, and D. Fuchs, *ibid.* **46**, 4483 (1992).
 - ¹¹ D.S. Falk, Phys. Rev. **118**, 105 (1960).
 - ¹² G.S. Painter, D.E. Ellis, and A.R. Lubinsky, Phys. Rev. B **4**, 3610 (1971).
 - ¹³ J.A. Van Vechten and R.M. Martin, Phys. Rev. Lett. **28**, 446 (1972) [**28**, 646(E) (1972)].
 - ¹⁴ V.I. Gavrilenko and F. Bechstedt, Phys. Rev. B **54**, 13416 (1996).
 - ¹⁵ W. Käferböck, W. Rössler, V. Necas, P. Bauer, M. Peñalba, E. Zarate, and A. Arnau, Phys. Rev. B **55**, 13275 (1997). Note that their theoretical values are already multiplied with charge state fractions; the H⁺ curve in their Fig. 1 is not the analogue of our results.
 - ¹⁶ R.J. Mathar, J.R. Sabin, and S.B. Trickey, 18th Werner Brandt Workshop on Charged Particle Penetration Phenomena, June 4–5, 1998, Gainesville, FL (unpublished).
 - ¹⁷ J.D. Jackson and R.L. McCarthy, Phys. Rev. B **6**, 4131 (1972).
 - ¹⁸ U. Littmark and J.F. Ziegler, Phys. Rev. A **23**, 64 (1981).
 - ¹⁹ J.R. Sabin and J. Oddershede, Nucl. Instrum. Methods B **24/25**, 339 (1987).
 - ²⁰ H. Paul and J. Sacher, At. Data Nucl. Data Tables **42**, 105 (1989).
 - ²¹ The experimental value is -285 eV: J. Nithianandam and J.C. Rife, Phys. Rev. B **47**, 3517 (1993); Y. Ma, N. Wassdahl, P. Skytt, J. Guo, J. Nordgren, P. D. Johnson, J.-E. Rubensson, T. Boske, W. Eberhardt, and S.D. Kevan, Phys. Rev. Lett. **69**, 2598 (1992).
 - ²² R.W.N. Nilen, S.H. Connell, D.T. Britton, C.G. Fischer, E.J. Sendezera, P. Schaaff, W.G. Schmidt, J.P.F. Sellschop, and W.S. Verwoerd, J. Phys. Condens. Matter **9**, 6323 (1997).
 - ²³ M.-Z. Huang and W.Y. Ching, Phys. Rev. B **47**, 9449 (1993).
 - ²⁴ J. Lindhard and A. Winther, K. Dan. Vidensk. Selsk. Mat. Fys. Medd. **34**, No. 4 (1964).
 - ²⁵ J.F. Janni, At. Data Nucl. Data Tables **27**, 147 (1982).
 - ²⁶ T. Kaneko, At. Data Nucl. Data Tables **53**, 271 (1993).

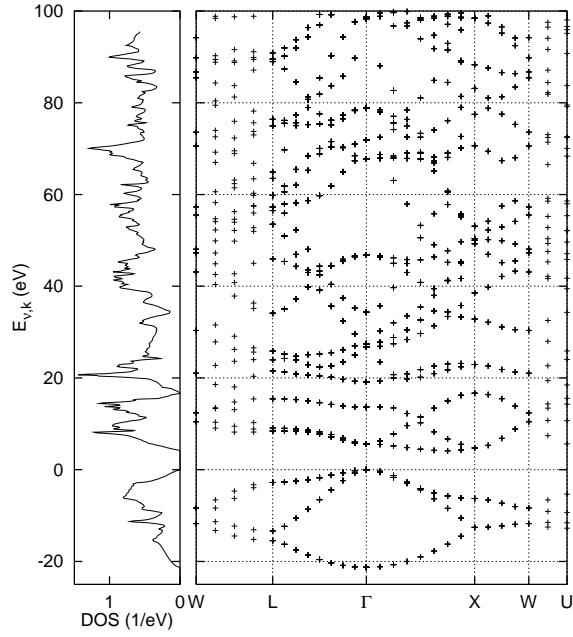


FIG. 1: KS band-structure $E_{\nu, \mathbf{k}}$ using $16 \times 16 \times 16$ \mathbf{k} -points in the BZ (213 in the IBZ). The direct gap at Γ is 5.59 eV, the indirect gap 4.13 eV, and the width of the four valence bands with eight electrons 21.29 eV. The two bands with four core electrons at -263 eV are not shown.²¹

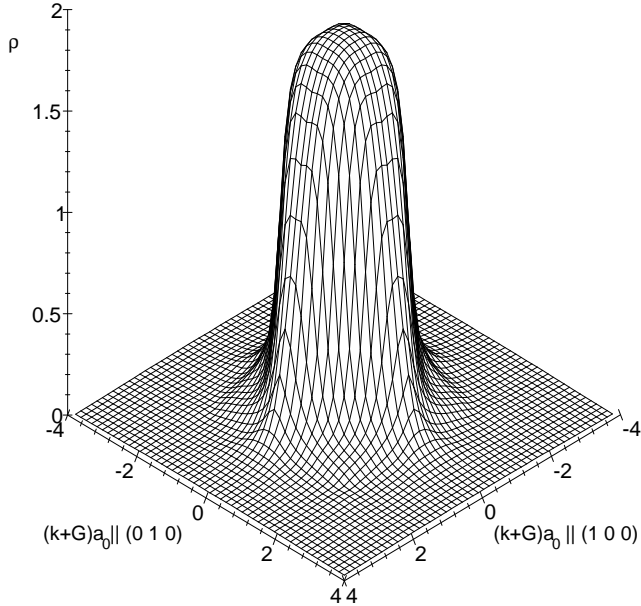


FIG. 2: The EMD as a function of $\mathbf{k} + \mathbf{G}$, which is varied in the plane spanned by (100) and (010). Both momentum components are measured in units of $1/a_0$. Anisotropies of “projected” positron-EMD’s are discussed in Ref. 22.

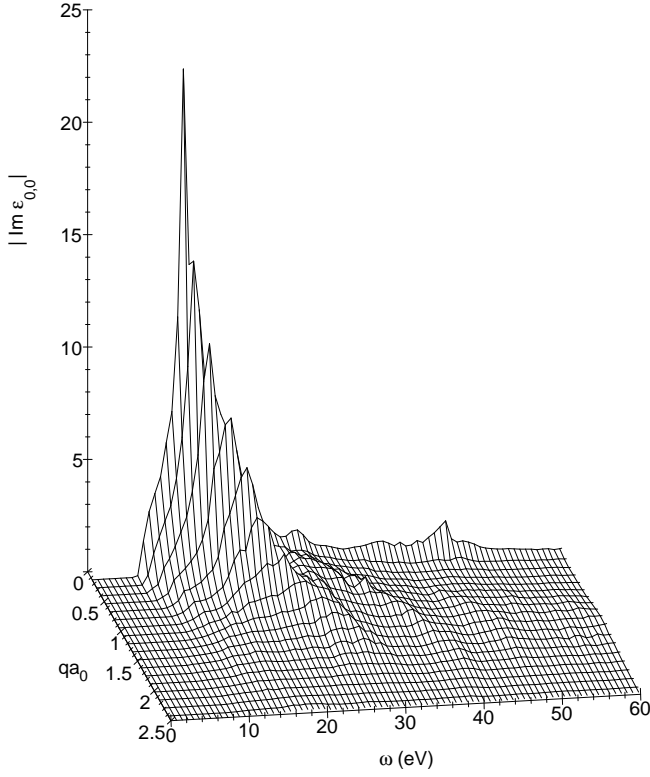


FIG. 3: Calculated $\text{Im}\epsilon_{\mathbf{G},\mathbf{G}'}$ for $\mathbf{G} = \mathbf{G}' = \mathbf{0}$ and $\mathbf{q} \parallel (\bar{1}11)$. The underlying DFT calculation is based on a $12 \times 12 \times 12$ mesh of \mathbf{k} -points in the BZ (98 points in the IBZ), which creates for this particular \mathbf{q} -direction commensurate values at $|\mathbf{q}| = (j/12)2\pi\sqrt{3}/a$ as shown here for $j = 1, 2, 3, \dots$

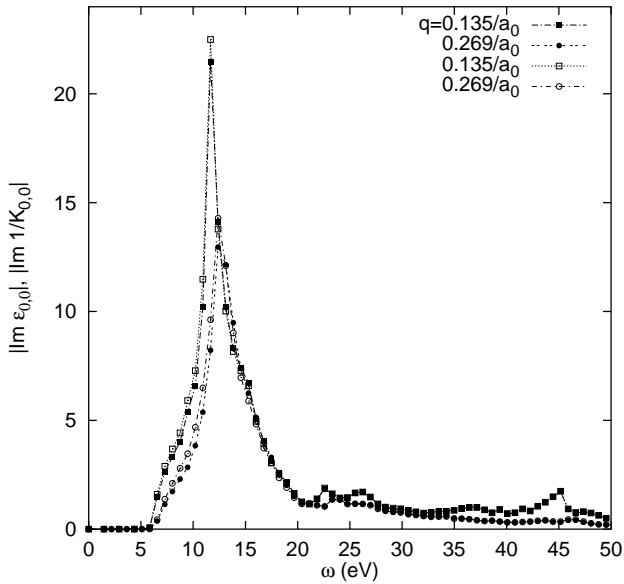


FIG. 4: The absolute value of $\text{Im}\epsilon_{0,0}(\mathbf{q}, \omega)$ (open symbols) and of $\text{Im}1/K_{0,0}(\mathbf{q}, \omega)$ (filled symbols). \mathbf{q} is parallel to $(\bar{1}11)$ with $qa_0 = 0.135$ ($j = 1$, squares) and $qa_0 = 0.269$ ($j = 2$, circles) as in Fig. 3. Note that Refs. 13,14 and 23 refer to the optical limit $q = j = 0$.

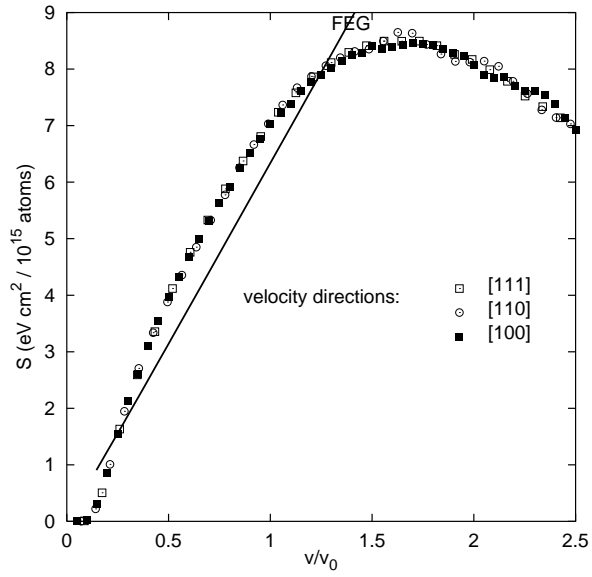


FIG. 5: Electronic stopping cross section of diamond. The stopping power was integrated on a mesh with 72 points on the ω -axis ($0 \dots 103$ eV). The lowest 28 bands were included in the sum over band-pairs in Eq. (2). The line refers to the free electron gas²⁴ with a density equivalent to 4 electrons per diamond atom.

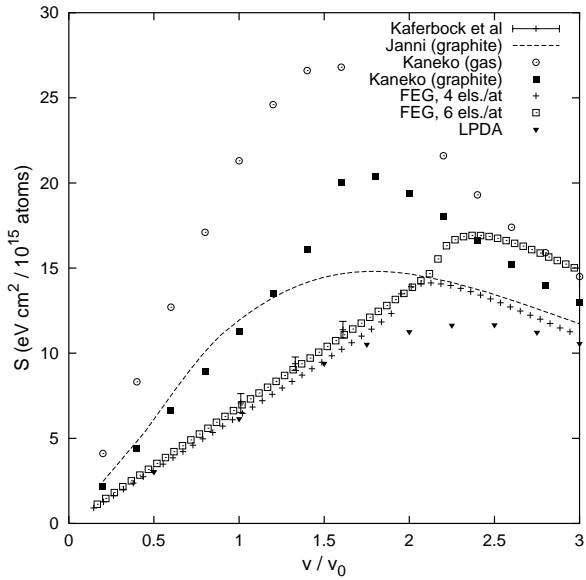


FIG. 6: Experimental proton stopping cross section by Käferböck *et al.*¹⁵ and of graphite by Janni,²⁵ compared with calculated values for gaseous carbon and solid graphite from Kaneko's theory,²⁶ and RPA free electron gas (FEG) values²⁴ with a homogeneous density equivalent to 4 or 6 electrons per diamond atom (Fermi velocity $1.457v_0$ or $1.668v_0$) as shown.